Bioorganic & Medicinal Chemistry 22 (2014) 2311–2319

Contents lists available at ScienceDirect

Bioorganic & Medicinal Chemistry

journal homepage: www.elsevier.com/locate/bmc

Synthesis, biological evaluation and 3D-QSAR studies of new chalcone derivatives as inhibitors of human P-glycoprotein

Zahida Parveen [a,c,†], Gerda Brunhofer [b,†], Ishrat Jabeen [b,†], Thomas Erker [b], Peter Chiba [a], Gerhard F. Ecker [b,*]

[a] Institute of Medical Chemistry, Medical University Vienna, Waehringer Strasse 10, 1090 Vienna, Austria
[b] University of Vienna, Department of Medicinal Chemistry, Althanstrasse 14, 1090 Vienna, Austria
[c] Abdul Wali Khan University Mardan, Malakand Mardan Rd, Mardan, Pakistan

ARTICLE INFO

Article history:
Received 2 December 2013
Accepted 6 February 2014
Available online 15 February 2014

Keywords:
ABCB1
MDR
P-glycoprotein
Chalcones
GRIND

ABSTRACT

P-glycoprotein (P-gp) is an ATP-dependent multidrug resistance efflux transporter that plays an important role in anticancer drug resistance and in pharmacokinetics of medicines. Despite a large number of structurally and functionally diverse compounds, also flavonoids and chalcones have been reported as inhibitors of P-gp. The latter share some similarity with the well studied class of propafenones, but do not contain a basic nitrogen atom. Furthermore, due to their rigidity, they are suitable candidates for 3D-QSAR studies. In this study, a set of 22 new chalcone derivatives were synthesized and evaluated in a daunomycin efflux inhibition assay using the CCRF.CEM.VCR1000 cell line. The compound **10** showed the highest activity (IC_{50} = 42 nM), which is one order of magnitude higher than the activity for an equilipohillic propafenone analogue. 2D- and 3D-QSAR studies indicate the importance of H-bond acceptors, methoxy groups, hydrophobic groups as well as the number of rotatable bonds as pharmacophoric features influencing P-gp inhibitory activity.

© 2014 Published by Elsevier Ltd.

1. Introduction

Human P-glycoprotein (ABCB1, P-gp) is a multispecific drug efflux transporter which mediates resistance of cancer cells to cytotoxic drugs.[1] It belongs to the family of ATP-binding cassette transport proteins that protect cells from the toxic effect of compounds through active outward transfer.[2] It has been demonstrated in animal models, that even low levels of expression can cause resistance of tumors to cytotoxic drugs. Early on, the concept of simultaneous administration of anticancer drugs with inhibitors of P-gp has been advocated as a concept for evading resistance. However, clinical studies have not lived up to the high expectations, and several phase II and phase III clinical studies have been terminated prematurely because of severe side effects related to P-gp inhibition.

Nevertheless, a proof-of-concept study illustrated that co-administration of the anticancer agent topotecan and elacridar, an inhibitor of both P-gp and BCRP (ABCG2, breast cancer resistance protein), significantly increased the bioavailability of the anticancer drug and reduced inter-patient variability.[3] In order to find more potent ABC transporter inhibitors, natural products often provide interesting scaffolds and serve as lead structures, as recently reviewed by Klepsch et al.[4] Flavonoids, polyphenolic compounds found to be ubiquitous in the plant kingdom, have been shown to possess inhibitory activity towards BCRP.[5] In case of P-gp, Zhang and colleagues reported that quercetin, genistein, and morin had inhibitory activity towards P-gp mediated daunomycin transport.[6] Recently, a QSAR model based on naturally occurring flavonoids was published describing their modulating effect on P-gp.[7]

For chalcones, which are biosynthetic precursors of flavonoids, detailed structure activity relationship information with respect to their interaction with P-gp is still missing. Chalcones used in this study contain delocalized pi-electron systems, which restrain structural flexibility and may be regarded as planar and linear, which renders them suitable candidates for 3D-QSAR studies. Furthermore, the chalcones reported in this study are structurally related to a set of propafenones previously studied by our group. However, chalcones are more rigid and are uncharged compounds, as they lack protonable nitrogens. Another important feature associated with these compounds is that they are photoactivable and can be used as tool compounds to label P-gp. Finally, similar to the structurally related flavonoids, chalcones are described to possess both P-gp and BCRP inhibitory properties. Recent studies

* Corresponding author. Tel.: +43 4277 55110; fax: +43 4277 9551.
E-mail address: gerhard.f.ecker@univie.ac.at (G.F. Ecker).
† Z.P., G.B., and I.J. contributed equally to this work.

http://dx.doi.org/10.1016/j.bmc.2014.02.005
0968-0896/© 2014 Published by Elsevier Ltd.

showed that basic as well as non-basic chalcone derivatives modulate ABC transporters.[8–10] These data together with those presented herein suggest that chalcones offer a new compound class which can be used to restore sensitivity of cells to chemotherapeutic agents (chemo-sensitizers).

2. Experimental procedure

2.1. Chemistry

Unless otherwise stated, all chemicals were obtained from Sigma–Aldrich or TCI Europe and were of analytical grade. Melting points were determined on a Kofler hot stage apparatus and are uncorrected. The ^{1}H and ^{13}C NMR spectra were recorded on a Bruker Avance DPx200 (200 and 50 MHz). Chemical shifts are reported in δ units (ppm) relative to Me_4Si line as internal standard and J values are reported in Hertz. Mass spectra were obtained by a Hewlett Packard (GC: 5890; MS: 5970) spectrometer. The purity of the synthesized compounds was established by combustion analysis with a Perkin-Elmer 2400 CHN elemental analyzer and was within ±0.4%. Solutions in organic solvents were dried over anhydrous sodium sulphate.

2.1.1. General synthesis procedure for compounds 1 and 2

To a suspension of 5 mmol of the corresponding benzaldehyde, 7.5 mmol (3.220 g) (1,3-dioxolan-2-yl-methyl)triphenylphosphonium bromide and 0.005 g 18-crown-6 in anhydrous THF and under argon atmosphere 20.8 mmol (0,499 g) NaH were added carefully. The reaction mixture was stirred till the reaction was completed (monitoring by TLC). Then, the mixture was cooled to 0 °C and first water and then 10% HCl were carefully added. After 60 min stirring at room temperature, the mixture was extracted with ethyl acetate, 10% HCl and water. The combined organic phase was dried over Na_2SO_4 and the solvent was removed in vacuo. The so-obtained crude product was purified by flash chromatography.

2.1.1.1. (*E*)-2-Methylthiocinnamaldehyde (1) and 3,4,5-Trimethoxycinnamaldehyde (2). See Ref. 11.

2.1.2. General Synthesis Procedure for Compounds 3–23

A solution of the 2.5 mmol of the appropriate acetophenone, indanone, tetralone derivative or 1,3-diacteylbenzene and 2 mL 50% NaOH in 10 mL ethanol was stirred at room temperature for 30 min. Then, 2.5 mmol (or 5 mmol with 1,3-diacetylbenzene) of the corresponding benzaldehyde or cinnamaldehyde derivative, dissolved in 1 mL ethanol, were added and stirred at room temperature After conversion of the starting compounds was completed as monitored by TLC, the reaction mixture was poured into ice water and acidified with 10% HCl to pH 6. The so-formed solid was filtered off and the crude product was further purified by recrystallization in ethanol.

2.1.2.1. (*E*)-3-(2,4,6-Trimethylphenyl)-1-(2′-methoxyphenyl)-2-propen-1-one (3). See Ref. 12.

2.1.2.2. (*E*)-1-(3,4-Dimethoxyphenyl)-3-(4-methoxy-1-naphthyl)-2-propen-1-one (4). Yield: 0.174 g (20%) yellow solid; mp: 112–116 °C. **^{1}H** NMR ($CDCl_3$): **δ** 8.62 (AB-system, **J** = 15.3, 1H), 8.38–8.21 (m, 2H), 7.89 (d, **J** = 8.2 Hz, 1H), 7.77–7.49 (m, 5H), 7.00–6.84 (m, 2H), 4.05 (s, 3H), 3.99 (s, 3H), 3.97 (s, 3H). **^{13}C** NMR ($CDCl_3$): **δ** 188.6, 157.6, 153.1, 149.2, 141.0, 132.8, 131.6, 127.5, 126.0, 125.6, 124.8, 123.2, 122.9, 122.6, 121.9, 110.8, 110.0, 103.7, 56.1, 56.0, 55.7. MS ***m*/*z***: 348 (72%, M^+), 165 (100%), 158 (40%), 139 (91%), 79 (55%). Anal. Calcd for $C_{22}H_{20}O_4\times H_2O$: C, 75.45; H, 5.81. Found: C, 75.42; H, 5.90.

2.1.2.3. (2*E*,4*E*)-5-(2-Methoxypehnyl)-1-(3′,4′,5′-trimethoxyphenyl)-2,4-pentadien-1-one (5). Yield: 1.240 g (70%) of yellow crystals; mp: 111 °C. ^{1}H NMR ($CDCl_3$): δ 7.72–7.53 (m, 2H), 7.52–7.23 (m, 4H), 7.17–6.89 (m, 4H), 3.95 (s, 6H), 3.93 (s, 3H), 3.90 (s, 3H). ^{13}C NMR ($CDCl_3$): δ 189.2, 157.6, 153.0, 145.9, 142.1, 137.3, 133.7, 130.4, 127.4, 125.0, 124.3, 120.7, 111.1, 105.8, 60.9, 56.3, 55.5. MS *m*/*z*: 354 (100%, M^+), 339 (73%), 195 (28%), 140 (25%), 91 (54%). Anal. Calcd for $C_{21}H_{22}O_5\times 0.3H_2O$: C, 71.16; H, 6.26. Found: C, 70.91; H, 6.47.

2.1.2.4. 5-(2-Methoxyphenyl)-1-(4′-hydroxy-3′,5′-dimethoxyphenyl)-2,4-pentadien-1-one (6). Yield: 0.240 g (28%) yellow solid; mp: 44–51 °C. ^{1}H NMR ($CDCl_3$): δ 7.78–6.87 (m, 10H), 5.99 (s, broad, 1H), 3.98 (s, 6H), 3.90 (s, 3H). ^{13}C NMR ($CDCl_3$): δ 188.6, 157.5, 146.8 (2C), 145.4, 139.3, 137.0, 130.3, 129.9, 127.5, 127.4, 125.1, 124.2, 120.7, 111.1, 105.7(2C), 56.5 (2C), 55.5. MS *m*/*z*: 340 (100%, M^+), 309 (8%), 246 (6%), 181 (35%), 115 (63%). Anal. Calcd for $C_{20}H_{20}O_5\times 0.1H_2O$: C, 70.20; H, 5.95. Found: C, 70.13; H, 5.71.

2.1.2.5. (*E*)-3-(2-Methylthiophenyl)-1-(3′,4′,5′-trimethoxyphenyl)-2-propen-1-one (7). Yield: 0.496 g (64%) yellow crystals; mp: 83–86 °C. **^{1}H** NMR ($CDCl_3$): **δ** 8.22 (AB-system, **J** = 15.6 Hz, 1H), 7.71–7.59 (m, 1H), 7.48–7.27 (m, 6H), 3.95 (s, 6H), 3.94 (s, 3H), 2.50 (s, 3H). **^{13}C** NMR ($CDCl_3$): **δ** 189.8, 153.1 (2C), 142.3, 141.7, 139.9, 134.1, 133.3, 130.4, 127.3, 127.0, 125.5, 124.3, 106.2 (2C), 60.9, 56.3, 16.5. MS ***m*/*z***: 344 (1%, M^+), 297 (100%), 236 (5%), 195 (13%), 149 (88%). Anal. Calcd for **$C_{19}H_{20}O_4S$**: C, 66.26; H, 5.85. Found: C, 66.22; H, 5.91.

2.1.2.6. 5-(2-Methylthiophenyl)-1-(3′,4′,5′-trimethoxyphenyl)-2,4-pentadiene-1-one (8). Yield: 0.509 g (55%) yellow crystals. mp: 114.5–115.5 °C. **^{1}H** NMR ($CDCl_3$): **δ** 7.76–7.42 (m, 3 H), 7.40–6.86 (m, 7 H), 3.95 (s, 6H), 3.94 (s, 3H), 2.48 (s, 3H). **^{13}C** NMR ($CDCl_3$): **δ** 189.0, 153.1 (2C), 144.8, 142.3, 138.6, 138.3, 135.1, 133.4, 129.4, 128.4, 127.3, 126.2, 125.6, 125.2, 105.8 (2C), 60.9, 56.3 (2C), 16.5. MS: ***m*/*z*** 370 (M^+, 65%), 355 (46%), 297 (60%), 187 (100%), 149 (90%). Anal. Calcd for **$C_{21}H_{22}O_4S$**: C, 68.08; H, 5.99. Found: C, 67.74; H, 6.01.

2.1.2.7. 2-[1-(4-Dimethylaminophenyl)-methylidene]-5,6-dimethoxyindan-1-one (9). Yield: 0.457 g (57%) yellow crystals. mp: 196–203 °C. ^{1}H NMR ($CDCl_3$): δ 7.68–7.49 (m, 3H), 7.34 (s, 1H), 6.97 (s, 1H), 6.73 (d, J = 9.0 Hz, 2H), 3.99 (s, 3H), 3.95 (s, 3H), 3.90 (s, 2H), 3.04 (s, 6H). ^{13}C NMR ($CDCl_3$): δ 193.3, 154.7, 150.9, 149.4, 144.3, 133.3, 132.4 (2C), 131.7, 130.6, 123.4, 111.9 (2C), 107.2, 104.9, 56.2, 56.1, 40.7 (2C), 32.4. MS: *m*/*z* 323 (M^+, 100%), 280 (13%), 237 (14%), 161 (15%), 121 (20%). Anal. Calcd for $C_{20}H_{21}NO_3$: C, 74.28; H, 6.55; N, 4.33. Found: C, 74.07; H, 6.50; N, 4.25.

2.1.2.8. 2-[3-(4-Dimethylaminophenyl)-prop-2-en-yliden]-5,6-dimethoxyindan-1-one (10). Yield: 0.422 g (48%) orange crystals. mp: 210–213 °C. **^{1}H** NMR ($CDCl_3$): **δ** 7.50–7.29 (m, 4H), 7.02–6.61 (m, 5H), 3.99 (s, 3H), 3.93 (s, 3H), 3.72 (s, 2H), 3.01 (s, 6H). **^{13}C** NMR ($CDCl_3$): **δ** 192.5, 154.8, 150.9, 149.4, 143.8, 142.2, 134.1, 133.3, 132.7, 128.7 (2C), 124.6, 119.9, 112.0 (2C), 107.2, 104.8, 56.2, 56.1, 40.2 (2C), 30.2. MS: ***m*/*z*** 349 (M^+, 100%), 334 (17%), 175 (19%), 144 (25%), 117 (27%). Anal. Calcd for **$C_{22}H_{23}NO_3$**: C, 75.62; H, 6.64; N, 4.01. Found: C, 75.35; H, 6.60; N, 3.96.

2.1.2.9. 6-Methoxy-2-[1-naphthalen-2-yl-methylidene]-3,4-dihydro-2*H*-naphthalen-1-one (11). See Ref. 13.

2.1.2.10. 6,7-Dimethoxy-2-(3-(3,4,5-trimethoxyphenyl)-2-propenylidene)-1-tetralone (12). Yield: 0.282 g (27%) yellow solid.

mp: 89–94 °C. ^{1}H NMR ($CDCl_3$): δ 7.62 (s, 1H), 7.51 (AB-system, J = 10.4 Hz, 1H) 7.17–6.87 (m, 2H), 6.82–6.64 (m, 3H), 3.96 (s, 3H), 3.95 (s, 3H), 3.88 (s, 6H), 3.16–2.88 (m, 4H). ^{13}C NMR ($CDCl_3$): δ 186.1, 153.4, 153.3, 148.2, 140.4, 138.3, 135.1, 134.1, 132.4, 126.9, 122.9, 109.9, 109.5, 104.2 (2C), 61.0, 56.2 (2C), 56.0 (2C), 28.5, 26.3. MS: m/z 410 (M^+, 100%), 395 (37%), 379 (40%), 231 (35%), 175 (41%). Anal. Calcd for $C_{24}H_{26}O_6$: C, 70.23; H, 6.38. Found: C, 70.01; H, 6.39.

2.1.2.11. 6-Methoxy-2-(3-(3,4,5-trimethoxyphenyl)-2-propenylidene)-1-tetralone (13). Yield: 0.399 g (42%) yellow crystals. mp: 152–156 °C. ^{1}H NMR ($CDCl_3$): δ 8.10 (d, J = 8.7 Hz, 1H), 7.51 (AB-system, J = 10.2 Hz, 1H), 7.15–6.84 (m, 3H), 6.78–6.68 (m, 3H), 3.92 (s, 6H), 3.88 (s, 3H), 3.87 (s, 3H), 3.00 (s, 4H). ^{13}C NMR ($CDCl_3$): δ 186.2, 163.4, 153.4, 145.8, 140.5, 135.2, 134.3, 132.4, 130.6, 127.3, 122.9, 113.2, 112.4, 104.2 (2C), 61.0, 56.2 (2C), 55.4, 29.2, 26.1. MS: m/z 380 (M^+, 100%), 365 (46%), 349 (47%), 161 (69%), 115 (33%). Anal. Calcd for $C_{23}H_{24}O_5$: C, 72.61; H, 6.36. Found: C, 72.36; H, 6.31.

2.1.2.12. 6-Methoxy-2-(3-(3,4,5-trimethoxyphenyl)-2-propenylidene)-1-indanone (14). Yield: 0.445 g (49%) yellow crystals. mp: 182–186 °C. ^{1}H NMR ($CDCl_3$): δ 7.51–7.29 (m, 3H), 7.19 (dd, J = 8.3 Hz, J = 2.5 Hz, 1H), 7.02–6.82 (m, 2H), 6.74 (s, 2H), 3.93 (s, 6H), 3.89 (s, 3H), 3.86 (s, 3H), 3.84–3.78 (m, 2H). ^{13}C NMR ($CDCl_3$): δ 193.5, 159.5, 153.4, 141.9, 141.6, 140.5, 136.7, 133.2, 131.9, 126.9, 123.7, 123.7, 105.6, 104.4 (2C), 61.0, 56.2 (2C), 55.6, 29.8. MS: m/z 366 (M^+, 100%), 351 (44%), 335 (46%), 165 (24%), 82 (24%). Anal. Calcd for $C_{22}H_{22}O_5$: C, 72.12; H, 6.05. Found: C, 71.85; H, 6.04.

2.1.2.13. 6,7-Dimethoxy-2-(3-(3,4,5-trimethoxyphenyl)-2-propenylidene)-1-indanone (15). Yield: 0.709 g (72%) yellow crystals. mp: 193–195 °C. ^{1}H NMR ($CDCl_3$): δ 7.39–7.29 (m, 2H), 6.99–6.87 (m, 3H), 6.73 (s, 2H), 3.99 (s, 3H), 3.93 (s, 9H), 3.89 (s, 3H), 3.78 (s, 2H). ^{13}C NMR ($CDCl_3$): δ 182.4, 155.2, 153.4, 149.5, 144.0, 141.1, 136.5, 132.4, 132.1, 131.7, 123.8, 107.2, 104.9, 104.3 (2C), 61.0, 56.2, 56.2 (2C), 56.1, 30.1. MS: m/z 396 (M^+, 100%), 381 (36%), 365 (52%), 175 (22%), 165 (25%). Anal. Calcd for $C_{23}H_{24}O_6$: C, 69.68; H, 6.10. Found: C, 69.44; H, 6.05.

2.1.2.14. 6,7-Dimethoxy-2-(3-(4-hydroxy-3-methoxyphenyl)-2-propenylidene)-1-indanone (16). Yield: 0.559 g (64%) yellow crystals. mp: 114–120 °C. ^{1}H NMR ($CDCl_3$): δ 7.41–7.28 (m, 2H), 7.19–7.05 (m, 1H), 7.03–6.69 (m, 5H), 5.87 (s, 1H), 3.99 (s, 3H), 3.96 (s, 3H), 3.94 (s, 3H), 3.76 (s, 2H). ^{13}C NMR ($CDCl_3$): δ 192.5, 155.1, 149.5, 146.9, 146.7, 144.0, 141.4, 135.6, 132.4, 132.4, 129.1, 122.2, 121.3, 114.8, 109.1, 107.2, 104.9, 56.2, 56.1, 55.9, 30.1. MS: m/z 352 (M^+, 100%), 337 (34%), 335 (25%), 176 (16%), 101 (21%). Anal. Calcd for $C_{21}H_{20}O_5 \times 0.2H_2O$: C, 70.85; H, 5.78. Found: C, 70.67; H, 5.71.

2.1.2.15. 5-Methoxy-2-(3-(2-methoxyphenyl)-2-propenylidene)-1-indanone (17). Yield: 0.490 g (64%) orange crystals. mp: 151–154 °C. ^{1}H NMR ($CDCl_3$): δ 7.80 (d, J = 8.5 Hz, 1H), 7.56 (dd, J = 7.8 Hz, J = 1.5 Hz, 1H), 7.44–7.25 (m, 3H), 7.15–6.85 (m, 5H), 3.89 (s, 6H), 3.78 (s, 2H). ^{13}C NMR ($CDCl_3$): δ 192.2, 164.9, 157.4, 151.8, 136.5, 135.9, 133.1, 131.8, 130.2, 127.3, 125.8, 125.4, 124.9, 120.7, 115.0, 111.1, 109.7, 55.6, 55.5, 30.5. MS: m/z 306 (M^+, 100%), 199 (37%), 145 (30%), 115 (26%), 101 (22%). Anal. Calcd for $C_{20}H_{18}O_3$: C, 78.41; H, 5.29. Found: C, 78.14; H, 5.98.

2.1.2.16. 4-[(*E*)-3-Oxo-3-(3′,4′,5′-trimethoxyphenyl)-1-propenyl] benzoic acid (18). Yield: 0.445 g (52%) yellow crystals. mp: 223 °C. ^{1}H NMR (DMSO-d_6): δ 13.1 (s, 1H), 8.08 (AB-system J = 15.7 Hz, 1H), 8.01 (s, 4H), 7.78 (AB-system J = 15.7 Hz, 1H), 7.45 (s, 2H), 3.90 (s, 6H), 3.77 (s, 3H). ^{13}C NMR (DMSO-d_6): δ 187.3, 166.4, 152.5, 142.0, 141.7, 138.3, 132.2, 131 6, 129.2, 128.5, 123.5, 105.8, 59.7, 55.7. MS: m/z 342 (M^+, 100%), 327 (29%), 299 (24%), 195 (47%), 103 (26%). Anal. Calcd for $C_{19}H_{18}O_6$: C, 66.66; H, 5.30. Found: C, 66.52; H, 5.28.

2.1.2.17. 4-[(*E*)-3-Oxo-3-ferrocenyl-1-propenyl]benzoic acid (19). Yield: 0.405 g (45%) red crystals. mp: >350 °C. ^{1}H NMR (DMSO-d_6): δ 13.12 (s, broad, 1H), 8.30–7.82 (m, 4H), 7.67 (AB-system, J = 15.6 Hz, 1H), 7.53 (AB-system, J = 15.6 Hz, 1H), 5.07 (s, 2H), 4.68 (s, 2H), 4.22 (s, 5H). ^{13}C NMR (DMSO-d_6): δ 192.1, 158.4, 139.3, 138.6 (2C), 131.9, 128.9, 126.0 (2C), 80.7, 73.2 (2C), 70.0 (5C), 69.9 (2C). MS: m/z 360 (M^+, 100%), 165 (76%), 121 (33%), 102 (15%), 56 (28%). Anal. Calcd for $C_{20}H_{16}O_3Fe$: C, 66.69; H, 4.48. Found: C, 66.43; H, 4.23.

2.1.2.18. 1-(3,4-Dimethoxyphenyl)-3-[3-(3,4-dimethoxyphenyl)-3-oxo-1-propenyl]phenyl)-2-propen-1-one (20). Yield: 0.161 g (14%) pale yellow solid. mp: 121–125 °C. ^{1}H NMR ($CDCl_3$): δ 7.95–7.79 (m, 3H), 7.76–7.57 (m, 8H), 7.56–7.44 (m, 1H), 6.95 (d, J = 8.3 Hz, 2H), 3.99 (s, 12H). ^{13}C NMR ($CDCl_3$): δ 188.2 (2C), 153.4 (2C), 149.3 (2C), 143.0 (2C), 135.8 (2C), 131.1 (2C), 129.8 (2C), 129.5, 128.3, 123.1 (2C), 122.5 (2C), 110.7 (2C), 110.0 (2C), 56.1 (2C), 56.1 (2C). MS: m/z 458 (M^+, 54%), 293 (51%), 165 (100%), 137 (17%), 77 (26%). Anal. Calcd for $C_{28}H_{26}O_6 \times 0.5H_2O$: C, 71.93; H, 5.82. Found: C, 71.82; H, 6.05.

2.1.2.19. 3-{3-[3-Oxo-3-(3,4,5-trimethoxyphenyl)-1-propenyl] phenyl}-1-(3,4,5-trimethoxyphenyl)-2-propen-1-one (21). Yield: 0.519 g (40%) white solid. mp: 152–154 °C. ^{1}H NMR ($CDCl_3$): δ 77.94–7.80 (m, 3H), 7.72 (dd, J = 7.6 Hz, J = 1.3 Hz, 2H), 7.61–7.47 (m, 3H), 7.30 (s, 3H), 3.97 (s, 12H), 3.95 (s, 6H). ^{13}C NMR ($CDCl_3$): δ 188.9 (2C), 153.2 (4C), 143.6 (2C), 135.7 (4C), 133.2 (2C), 129.8 (2C), 129.6, 128.7, 122.6 (2C), 106.1 (4C), 61.0 (2C), 56.4 (4C). MS: m/z 518 (M^+, 100%), 323 (36%), 195 (95%), 152 (24%), 136 (23%). Anal. Calcd for $C_{30}H_{30}O_8$: C, 69.49; H, 5.83. Found: C, 69.19; H, 5.85.

2.1.2.20. (*E*)-3-(3,4,5-Trimethoxyphenyl)-1-{3-[(*E*)-3-(3,4,5-trimethoxyphenyl)-2-propenoyl]phenyl}-2-propen-1-one (22). Yield: 0.052 g (4%) pale yellow solid. mp: 145–148 °C. ^{1}H NMR ($CDCl_3$): δ 8.63 (s, 1H), 8.23 (dd, J = 7.7 Hz, J = 1.6 Hz, 2H), 7.78 (AB-system, J = 15.5 Hz, 2H), 7.67 (t, J = 7.7 Hz, 2H), 7.46 (AB-system, J = 15.5 Hz, 2H), 6.90 (s, 4H), 3.94 (s, 12H), 3.92 (s, 6H). ^{13}C NMR ($CDCl_3$): δ 189.8 (2C), 153.5 (4C), 146.0 (2C), 138.7 (2C), 132.3 (2C), 130.0 (2C), 129.0, 128.2, 120.8 (2C), 105.8 (4C), 61.0 (2C), 56.1 (4C). MS: m/z 518 (M^+, 100%), 487 (38%), 221 (33%), 206 (20%), 193 (15%). Anal. Calcd for $C_{30}H_{30}O_8 \times 0.1H_2O$: C, 69.25; H, 5.85. Found: C, 69.06; H, 5.92.

2.1.2.21. 5-(3,4,5-Trimethoxyphenyl)-1-{3-[5-(3,4,5-trimethoxyphenyl)-2,4-pentadienoyl]phenyl}-2,4-pentadien-1-one (23). Yield: 0.271 g (19%) yellow solid. mp: 142–145 °C. ^{1}H NMR ($CDCl_3$): δ 8.57 (s, 1H), 8.18 (dd, J = 7.8 Hz, J = 1.5 Hz, 2H), 7.78–7.54 (m, 3H), 7.17 (AB-system, J = 14.8 Hz, 2H), 7.06–6.91 (m, 4H), 6.75 (s, 4H), 3.92 (s, 12H), 3.89 (s, 6H). ^{13}C NMR ($CDCl_3$): δ 189.5 (2C), 153.4 (4C), 145.4 (2C), 142.5 (2C), 139.5 (2C), 138.5 (2C), 132.2 (2C), 131.6 (2C), 129.0, 128.1, 126.3 (2C), 124.6 (2C), 104.5 (4C), 61.0 (2C), 56.1 (4C). MS: m/z 570 (M^+, 4%), 218 (100%), 204 (19%), 188 (55%), 117 (27%). Anal. Calcd for $C_{34}H_{34}O_8 \times 0.3H_2O$: C, 70.89; H, 6.08. Found: C, 70.80; H, 6.00.

2.1.2.22. Methyl-2-hydroxy-3-[3-(2-methoxyphenyl)-prop-2-enyliden]cyclohexene-1-carboxylate (24). The compound was synthesized according to the procedure described previously:[14] to a solution of 10 mmol (1.702 g, 1.6 mL) ethyl 2-cyclohexanone carboxylate and 10 mmol (1.522 g, 1.5 mL) diazabicycloundecene (DBU) in 20 mL dry methanol 10 mmol (1.622 g) 2-methoxycinnamicaldehyde, dissolved in 10 mL dry methanol, added. The

reaction mixture stirred under argon atmosphere at room temperature for 40 hours. Then, it was cooled to 0 °C, the obtained precipitate was filtered off and recrystallized in ethanol. Yield: 0.599 g (20%) yellow crystals. mp: 125–128 °C. ^{1}H NMR ($CDCl_3$): δ 12.22 (s, 1H), 7.52 (dd, J = 7.7 Hz, J = 1.5 Hz, 1H), 7.36–7.09 (m, 4H), 7.05–6.81 (m, 2H), 3.87 (s, 3H), 3.79 (s, 3H), 2.70–2.52 (m, 2H), 2.50–2.35 (m, 2H), 1.88–1.67 (m, 2H). ^{13}C NMR ($CDCl_3$): δ 173.2, 165.1, 157.1, 132.1, 130.4, 130.0, 129.2, 126.9, 126.2, 124.7, 120.7, 111.0, 99.6, 55.5, 51.6, 25.7, 23.2, 22.1. MS: m/z 300 (M^+, 57%), 268 (100%), 209 (13%), 134 (60%), 91 (47%). Anal. Calcd for $C_{18}H_{20}O_4$: C, 71.98; H, 6.71. Found: C, 71.96; H, 6.72.

2.2. Biological evaluation of chalcones

2.2.1. Cell lines

The resistant CCRF vcr1000 cell line was maintained in RPMI 1640 medium containing 10% fetal calf serum (FCS) and 1000 ng/mL vincristine. The selecting agent was washed out 1 week before the experiments. This cell line was selected due to its distinct P-gp expression.

2.2.2. Inhibition of daunorubicin efflux

IC_{50} values for daunorubicin efflux inhibition were determined as reported.[15] Briefly, cells were sedimented, the supernatant was removed by aspiration, and the cells were resuspended at a density of 1×10^6/mL in RPMI 1640 medium containing daunorubicin (Sigma Chemical Co., St. Louis, MO) at a final concentration of 3 μmol/L. Cell suspensions were incubated at 37 °C for 30 min. Tubes were chilled on ice and centrifuged at 500g in an Eppendorf 5403 centrifuge (Eppendorf, Hamburg, Germany). Supernatants were removed, and the cell pellet was resuspended in medium pre-warmed to 37 °C containing either no inhibitor or compounds at various concentrations ranging from 20 to 200 μM, depending on the solubility and expected potency of the inhibitor. Eight concentrations (serial 1:3 dilution) were evaluated for each inhibitor. After 60, 120, 180 and 240 s, aliquots of the incubation mixture were transferred to tubes containing an equal volume of ice-cold stop solution (RPMI medium containing GPV31 at a final concentration of 5 μmol/L). Zero time points were determined by immediately pipetting daunorubicin-preloaded cells into ice cold stop solution. Samples drawn at the respective time points were kept in an ice water bath and measured within 1 h on a Becton Dickinson FACSCalibur flow cytometer (Becton Dickinson, Vienna, Austria). Viable cells were selected by setting appropriate gates for forward and side scatter. The excitation and emission wavelengths were 482 nm and 558 nm, respectively. Five thousand gated events were accumulated for the determination of mean fluorescence values.

2.2.3. Mathematical model for determination of inhibitor IC_{50} values

Initial efflux rates were calculated from the time dependent linear decrease in mean flourescence through the use of linear regression analysis. IC_{50} values were determined from dose response curves of inhibitor concentration versus initial efflux rates. Data points were fitted according to the equation $V = V_0 - (V_0 - V_{inf}) \times [I]^n \div (IC_{50}^n + [I]^n)$ where V is the velocity of transport, V_0 is the transport velocity in the absence of inhibitor, V_{inf} is the efflux velocity at infinite concentration of inhibitor (which is equal to simple diffusion), $[I]$ is the inhibitor concentration, IC_{50} is the 50% inhibitory concentration (50% occupancy value) and n is the Hill coefficient.

2.3. Computational Models

2.3.1. GRID-Independent molecular descriptor analysis

Molecular discovery software Pentacle version 1.06 was used for computing alignment-independent 3D-descriptors.[16] This so called GRIND approach aims to extract the information enclosed in the molecular interaction fields (MIFs) and compress it into new types of variables whose values are independent of the spatial position of the molecule studied. Most relevant regions are extracted from the MIF by an optimization algorithm that uses the intensity of the field at a node and the mutual node-node distances between the chosen nodes as a scoring function. At each point, the interaction energy (*Exyz*) is calculated as a sum of Lennard–Jones energy (Elj), Hydrogen bond (Ehb) and Electrostatic (Eal) interactions.

$$Exyz = \sum Elj + \sum Eel + \sum Ehb$$

Default values for Grid Step (0.5 Å) and probes (DRY representing Hydrophobic interaction, O (Carbonyl Oxygen) representing hydrogen bond acceptor groups, N1 (Amide Nitrogen) representing H-bond donor groups and TIP representing a shape descriptor) were used for computation of the MIF. MIF discretization was performed by the AMANDA algorithm using default values for probe cutoff (DRY = −0.5, O = −2.6, N1 = −4.2, TIP = −0.74).[17] Nodes with an energy value below this cutoff were discarded. Large Auto and Cross Correlation (CLACC) algorithm was used for encoding the prefiltered nodes into GRIND thus producing most consistent variables as compared to MACC.[18]

QSAR. Molecular structures were built with the builder function of MOE[19] version 2010 and energy minimised. Partial charges were assigned by MMFF94 force field. 2D molecular descriptors, including atom and bond counts, connectivity indices, partial charge descriptors, pharmacophore feature descriptors and general physicochemical descriptors were calculated by using software MOE version 2010. PLS analysis was performed with the MOE QSAR model tool and the predictive ability of the models was determined by leave one out cross validation (LOO).

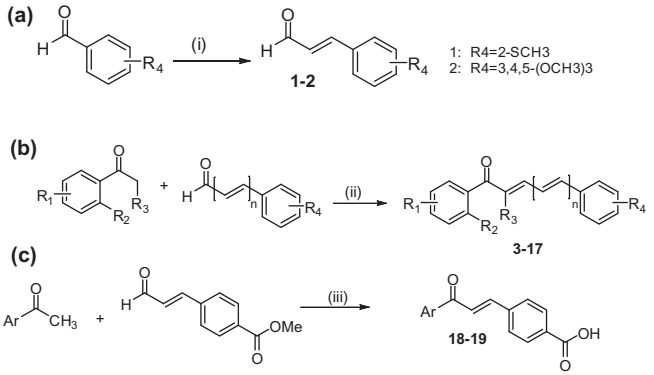

3: R1=2-OCH_3, R2=R3=H, R4=2,4,6-$(CH_3)_3$, n=0
4: R1=3,4-$(OCH_3)_2$, R2=R3=H, R4=2,3-(-CH=CH-CH=CH-), 4-OCH_3, n=0
5: R1=3,4,5-$(OCH_3)_3$, R2=R3=H, R4=2-OCH_3, n=1
6: R1=3,5-$(OCH_3)_2$, 4-OH, R2=R3=H, R4=2-OCH_3, n=1
7: R1=3,4,5-$(OCH_3)_3$, R2=R3=H, R4=2-SCH_3, n=0
8: R1=3,4,5-$(OCH_3)_3$, R2=R3=H, R4=2-SCH_3, n=1
9: R1=3,4-$(OCH_3)_2$, R2-R3=-CH_2-, R4=4-N$(CH_3)_2$, n=0
10: R1=3,4-$(OCH_3)_2$, R2-R3=CH_2, R4=4-N$(CH_3)_2$, n=1
11: R1=4-OCH_3, R2-R3=-CH_2-CH_2-, R4=3,4-(-CH=CH-CH=CH-), n=0
12: R1=3,4-$(OCH_3)_2$, R2-R3=-CH_2-CH_2-, R4=3,4,5-$(OCH_3)_3$, n=1
13: R1=4-OCH_3, R2-R3=-CH_2-CH_2-, R4=3,4,5-$(OCH_3)_3$, n=1
14: R1=3-OCH_3, R2-R3=-CH_2-, R4=3,4,5-$(OCH_3)_3$, n=1
15: R1=3,4-$(OCH_3)_2$, R2-R3=-CH_2-, R4=3,4,5-$(OCH_3)_3$, n=1
16: R1=3,4-$(OCH_3)_2$, R2-R3=-CH_2-, R4=3-OCH_3, 4-OH, n=1
17: R1=4-OCH_3, R2-R3=-CH_2-, R4=2-OCH_3, n=1

Scheme 1. Synthesis of (a) compounds **1**–**2**, (b) compounds **3**–**17** and (c) compounds **18** and **19**. Reagents and conditions: (i) (**1**) (1,3-dioxolan-2-ylmethyl)triphenylphosphonium bromide, NaH, 18-crown-6, THF, room temperature (**2**) 10% HCl, room temperature; (ii) 50% NaOH, EtOH, room temperature; (iii) (**1**) 50% NaOH, EtOH, room temperature, (**2**) 10% HCl, room temperature.

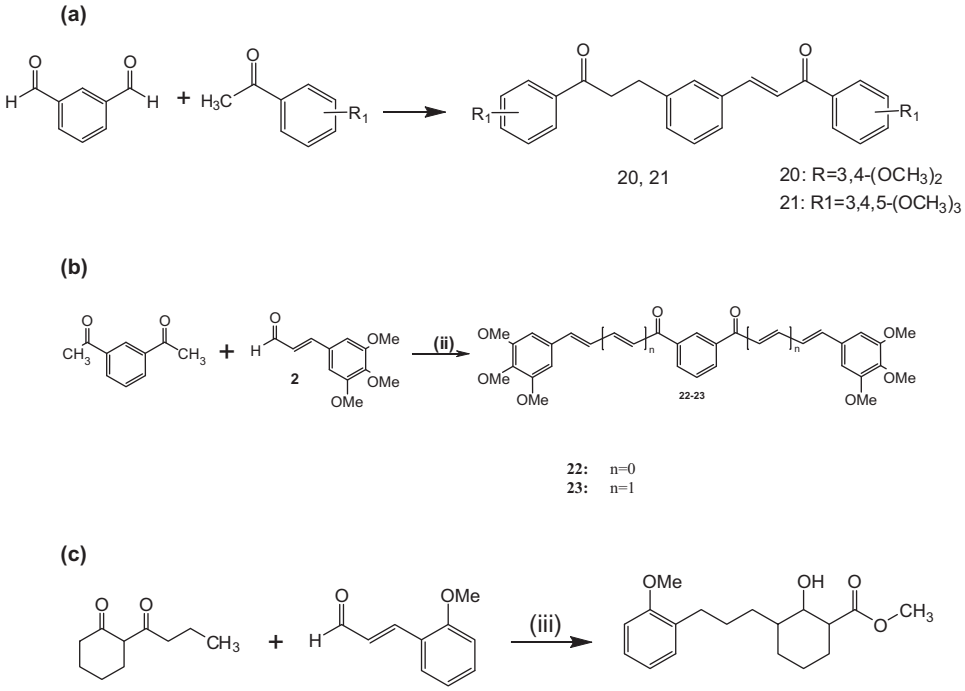

Scheme 2. Synthesis of (a) compounds **20**–**21**, (b) compounds **22**–**23** and (c) compound **24**. Reagents and conditions: (i), (ii) 50% NaOH, EtOH, room temperature; (iii) DBU, MeOH, argon, room temperature.

3. Results and discussion

3.1. Chemistry

Compounds **3**–**24** were synthesized as outlined in Schemes 1 and 2. All compounds are based on the chalcone scaffold, 1,3-diphenyl-2-propen-1-one, which was used as core structure. Substituents on both aromatic rings are mostly methoxy groups, which represent a pharmacophoric substructure for P-gp interaction.[20] But also derivatives bearing a combination of methoxy together with thiomethyl and tertiary amino groups showed high P-gp inhibitory activity. Further chemical variations concerned the length and type of the spacer linking the two phenyl rings (vinylogous and 'bridged' chalcones). The substances were obtained by base-catalyzed reaction of a corresponding acetophenone derivative with an appropriate cinnam- or benzaldehyde (Claisen–Schmidt condensation). Dimerising the core structure resulted in compounds **20**–**23**, which were received by the same procedure. Compound **19** is an example of a bioisosteric replacement of the phenyl part of compound 18 against a ferrocene feature which is a strategy often used in medicinal chemistry.[21,22] In compound **24**, one aromatic ring was exchanged by a cyclohexenol moiety. This compound was obtained by a DBU-methanol-promoted reaction of ethyl 2-cyclohexanone carboxylate and 2-methoxy cinnamaldehyde.[14]

Table 1
Biological activity (μM), pIC_{50} values, hydrophobic surface area (Vsa_hyd) and the number of rotatable bonds (b_rotN) for compounds **3**–**24**

Codes	IC_{50} (μM) ± SD[a]	pIC_{50}	Vsa_hyd	b_rotN
3	8.51 ± 1.50	5.07	269.85	4.00
4	2.75 ± 0.10	5.56	315.08	6.00
5	1.38 ± 0.59	5.86	338.97	8.00
6	12.0 ± 0.70	4.92	303.31	7.00
7	0.65 ± 0.15	6.19	318.56	7.00
8	0.87 ± 0.03	6.06	350.18	8.00
9	0.13 ± 0.07	6.87	298.03	4.00
10	0.04 ± 0.01	7.37	329.65	5.00
11	3.55 ± 0.33	5.45	262.88	2.00
12	0.14 ± 0.04	6.84	371.69	7.00
13	1.74 ± 0.38	5.76	343.39	6.00
14	1.15 ± 0.03	5.94	327.58	6.00
15	2.63 ± 2.25	5.58	355.89	7.00
16	2.33 ± 0.34	5.63	291.92	5.00
17	3.89 ± 0.40	5.41	270.96	4.00
18	141.30 ± 5.60	3.85	265.44	7.00
19	107.20 ± 8.40	3.97	192.15	4.00
20	0.14 ± 0.06	6.86	406.62	10.00
21	0.12 ± 0.07	6.92	463.23	12.00
22	0.14 ± 0.02	6.86	463.24	12.00
23	0.06 ± 0.01	7.24	526.47	14.00
24	20.4 ± 0.20	4.69	252.94	5.00

[a] Each IC_{50} determination was performed with eight concentrations, and each assay point was determined in triplicate.

3.2. Structure activity relationship

The whole data set covers a range of more than four orders of magnitude difference in biological activity, with indanone derivative 10 possessing highest biological activity (IC_{50}: 0.04 μM). Compounds **9** and **10**, which both contain an aniline nitrogen atom and only differ in one rotatable bond, showed a difference of 2-fold in their biological activity. A similar trend has been observed for compounds **20**–**23**, that are among the most active chalcone derivatives. They contain a similar substitution pattern on both sides of the central benzene ring, and differ in the number of rotatable bonds. Whereas almost no difference in biological activity exists between compounds **20**–**22**, compound **23** (IC_{50}: 0.06 μM), which possess two additional number of rotatable bonds, is about one order of magnitude more active than derivatives **20**–**22** (IC_{50}; 0.14: 0.12: 0.14 μM). We also synthesised indanones **14**–**17** and chalcone derivatives **3**–**8** and **11**–**13**, containing different numbers and pattern of methoxy groups. Almost no difference in biological activity of **15** and **16** has been identified. Overall, a minor difference (~factor of 1–2) exists in the indanones **14**–**17**. A similar

trend has been observed for chalcone derivatives, which indicates that a different number and pattern of methoxy groups on the indanone and chalcone scaffold and at the benzene ring on the opposite side of the molecules is not making any significant difference for biological activity. Compounds **18** and **19** are acidic analogs and comprise the least active compounds (IC_{50}: 141.30: 107.20) (Table 1).

3.3. 2D-QSAR

In order to identify the most relevant physicochemical features important for high P-gp inhibitory activity of chalcone analogs, multiple linear regression analysis was performed. Use of MOE's

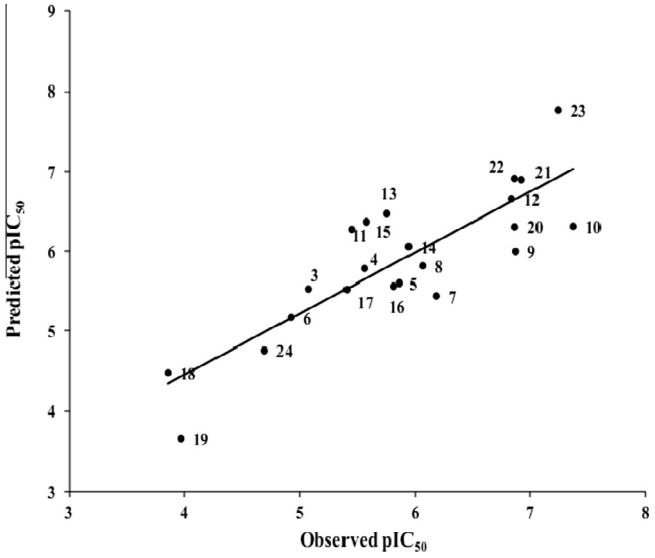

Figure 1. Plot of observed vs. predicted MDR-modulating activity of compounds **3**–**24**, predicted values were obtained by leave-one-out cross validation.

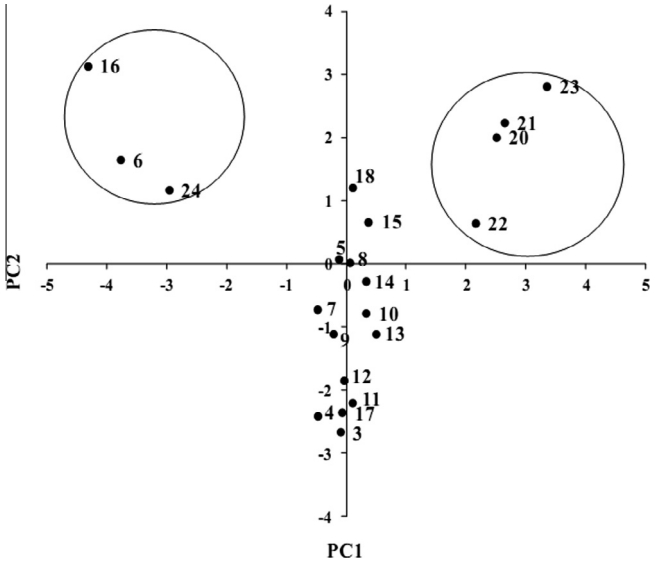

Figure 2. PCA score plot showing that the whole data set is divided into three groups; the upper right part contains flexible and large compounds, the lower portion contains less flexible and small compounds (mostly indanones and tetralones); the left part of the diagram contains all compounds having a hydrogen bond donor group.

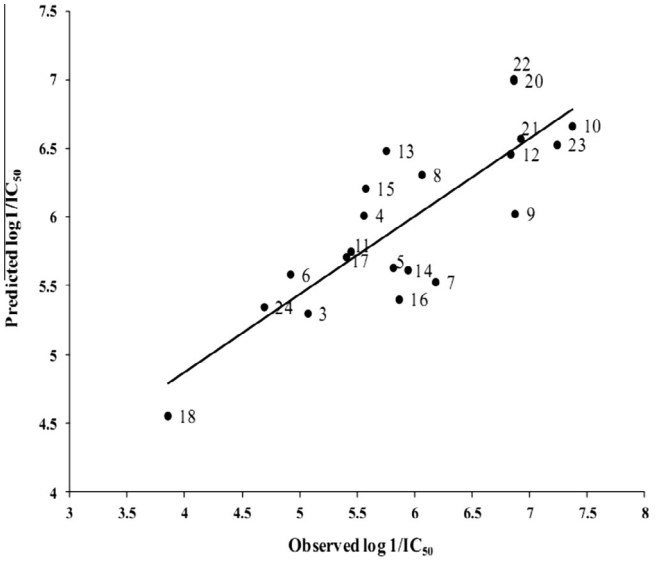

Figure 3. Plot of observed vs. predicted MDR activity (expressed as $\log(1/IC_{50})$ values) using the GRIND model.

contingency[23] analysis tool for identification of the most important descriptors revealed the following equation (Eq. (1)).

$$\text{Log}\ (1/IC_{50}) = 0.02\ (\text{vsa\_hyd}) - 0.36\ (\text{b\_rotN}) + 0.93 \qquad (1)$$

$$n = 22, R^2 = 0.79, q2(\text{LOO}) = 0.71, \text{RMSE} = 0.51.$$

Figure 5 shows a plot of observed vs biological activity predicted by QSAR Eq. 1. An excellent QSAR model was obtained with all predicted values within one order of magnitude from the measured ones. Descriptors contributing most to the variance in the biological activity comprised vsa_hyd and b_rotN (Eq. 1). This indicates that within this data set the number of rotatable bonds and the hydrophobic surface area are the most important structural attributes for high biological activity. This is in line with previous findings by Wang and colleagues, who showed that hydrophobic distribution within the molecules along with molecular weight, number of rotatable bonds and energy of highest occupied orbital (Ehomo) are important descriptors for P-gp inhibitory potency.[24] However, in our case the QSAR equation reveals a negative contribution of the number of rotatable bonds, which points towards an unfavorable entropic contribution.

Extensive QSAR studies on a large set of propafenone analogs revealed the importance of hydrogen bond acceptors and their strength, the distance between aromatic moieties and H-bond acceptors as well as the influence of global physicochemical parameters, such as lipophilicity and molar refractivity.[25–27] However, for the present data set of chalcone derivatives we identified only a poor correlation (r^2 = 0.18) between $c\log P$ and biological activity (Fig. 1). This indicates that the variance in the biological activity of chalcone derivatives is mainly driven by the concrete pattern of hydrophobicity distribution within the molecules, as represented by vsa_hyd, rather than by their ability to penetrate in the membrane bilayer. This is also in line with the findings of Pleban et al.[28] on the importance of the distribution of hydrophobicity within P-gp inhibitors. Later on this was further confirmed by König et al., by using hydrophobic moments as QSAR descriptors.[29] Finally, this is additionally supported by the recent X-ray structure of mouse P-gp, which shows a large inner cavity exhibiting several hydrophobic patches for space directed hydrophobic interactions.[30]

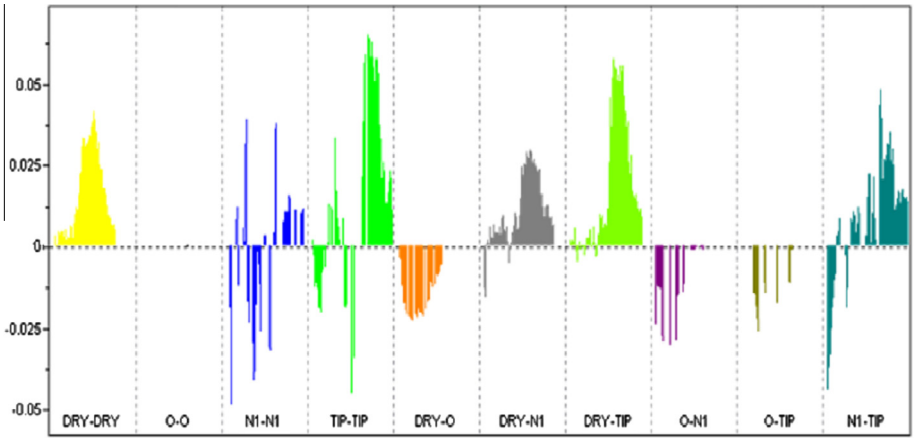

Figure 4. PLS Coefficient correlograms showing the descriptors which are directly (positive values) or inversely (negative values) correlated to the biological activity. The activity particularly increases with the increase in (DRY-DRY), (DRY-TIP) and (TIP-TIP) descriptor values.

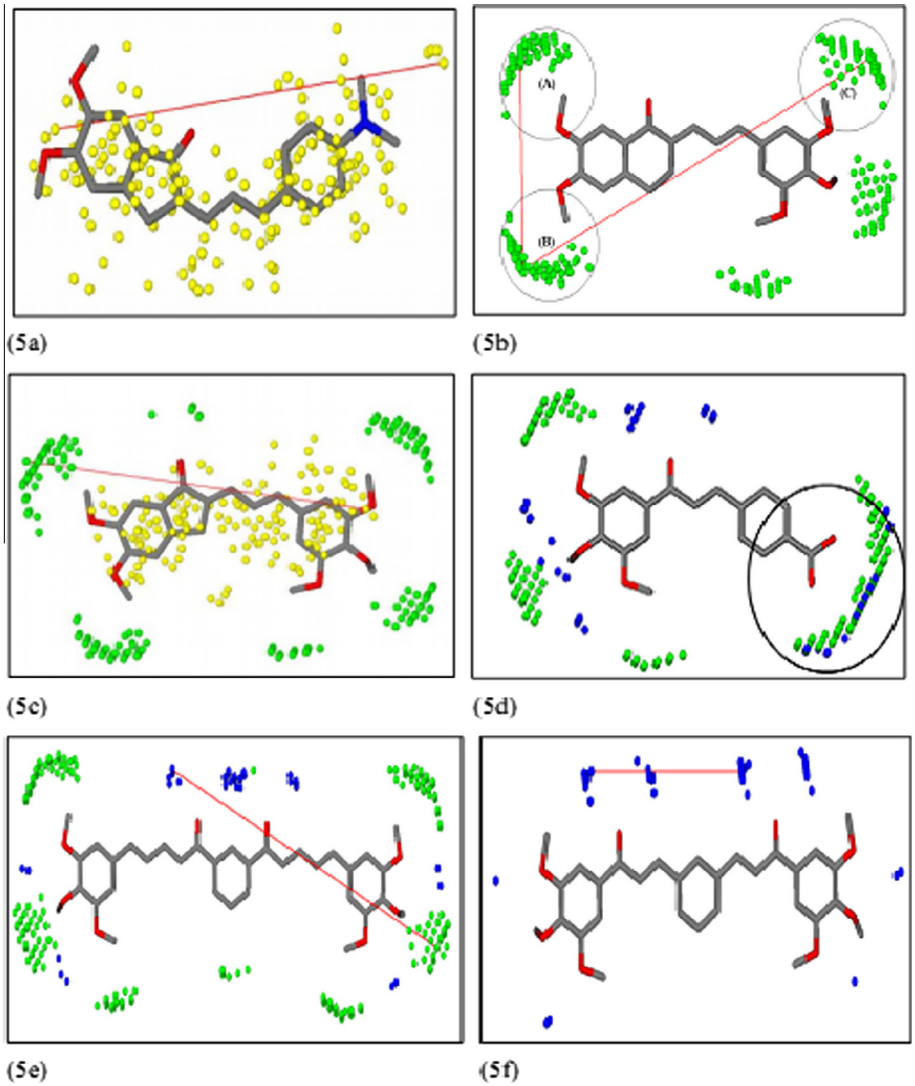

Figure 5. (a) DRY-DRY hot spots (yellow color) which represents two hydrophobic regions 16.00–16.40 Å apart, present in most active compounds. (b) Shows steric hot spots (green color) which makes three important boundaries (A, B and C) for most potent inhibitors of ABCB1 where A–B: 10.00–10.40 Å and A–C: 22.00–22.40 Å. (c) Represent the distance range of a hydrophobic substructure (yellow hot spot) from molecular extreme (A) (17.60–18.00 Å) (green hot spot). (d) Shows a carboxylic acid group (N1: blue hot spot) present very close (1.60–2.00 Å) to one of the molecular boundary (encircle), having negative effect to biological activity, while (e) represent the same pharmacophoric features at longer distance (20.80–21.20 Å) showing positive contribution towards biological activity. (f) N1–N1 hot spots (blue color) representing two H-bond acceptors at a distance of 9.20–9.60 Å which is favorable for biological activity of most of the compounds.

3.4. 3D-QSAR

Due to its rigid scaffold, chalcones represent versatile tools for 3D-QSAR studies. In recent years especially GRID-independent descriptors (GRIND) gained a lot of attraction in the field. GRIND descriptors are based on molecular interaction field (MIF) calculations and are alignment-independent, thus allowing the analysis of structurally diverse data series,[31] 23 3D conformations of the molecules in the data set were obtained from their 2D co-ordinates by using program CORINA[32] GRIND descriptors were derived by computing molecular interaction fields (MIF) and by identifying the regions with maximum field intensity at relative distances by using the AMANDA algorithm implemented in software Pentacle version 1.06.[33] The Consistently Large Auto and Cross Correlation (CLACC) algorithm was used for encoding the prefiltered nodes into GRIND. The values obtained from the analysis were represented directly in correlograms plots, where the product of node–node energies versus distance separating the nodes is reported.

First, the data set was examined using principal component analysis (PCA). The first two components explained 43% of the variance in the GRIND descriptors and separate the data mainly on basis of their pharmacophoric pattern (Fig. 2). Thus, compounds **6**, **16**, **24** in the upper left cluster share a similar pharmacophore having one hydrogen band donor (OH). Compounds **20**, **21**, **22**, **23** which contain two carbonyl groups and show higher flexibility, are located in the upper right hand side of the plot. Interestingly, acid **18**, which exhibits pharmacophoric features from both clusters (two C=O, one OH), is located almost in the middle of these two clusters. Compounds with negative PC values are relatively small (mostly indanones and tetralones) and contain one carbonyl group, 1–5 methoxy groups, but no hydrogen bond donor.

In order to analyze the underlying important pharmacophoric patterns, PLS multivariate data analysis correlating the biological activity with the complete set of GRIND variables (790) was carried out using the AMANDA algorithm.[31] The PLS analysis resulted in a two-latent variable model with an $r^2 = 0.85$. However, the cross-validation of the model yielded q^2 LOO values of 0.26, which is quite unsatisfying. Thus, to reduce the high number of variables, a variable selection was applied by using FFD factorial selection implemented in Pentacle.[33] The resulting number of active variables decreased from 523 to 422 which improved the quality of the model ($r^2 = 0.98$, q^2LOO = 0.66). Figure 3 shows the plot of the experimental versus predicted biological activities. Analysis of the PLS coefficients profile of the 3rd Latent Variable (LV) of the PLS model illustrates the identification of key descriptors for high biological activity (Fig. 4). Activity increases strongly with high value of the descriptors DRY-DRY, TIP-TIP, Dry-TIP, and N1-TIP (Table 2).

The GRIND model indicates the presence of two hydrophobic moieties, which are localized at two of the three steric hot spots identified, (Fig. 5a and b) in the most active (IC_{50} <1 μM) P-gp inhibitors. Most of the QSAR studies in the past two decades pointed towards the importance of hydrophobic substructures for high P-gp inhibitory potency.[25–27] Furthermore, by using a MIF-based pharmacophore model, Broccatelli et al recently provided also evidence for the importance of a distinct three dimensional shape of inhibitors of P-gp.[34]

Also our model elucidates the importance of an optimal shape of the ligands and identifies three important steric hot spots ('edges') A, B and C. In the molecules where hot spot (A) is 10.00–10.40 Å apart from (B), this represents two edges related to two methoxy substitutions at positions **6** and **7** of indanone and tetralone derivatives (Fig. 5b). However, in compounds **20**–**23**, which contain 3,4,5-tri methoxy groups, it represent the distance between the 3- and 4-annelated methoxy groups. The 3rd steric hot spot (C) represents the substituted benzene ring on the opposite side of the indanone and tetralone scaffold, which is at a distance of 22.00–22.40 Å from edge (A) in most of the active (IC_{50} <1 μM) compounds. This further confirms the importance of distinct 3D shape requirements for inhibitors of P-gp.

It seems that out of three identified steric hot spots, (A) represent the most favorable one as it serve as an anchor to measure the distances to a hydrophobic feature (Fig. 5c). Analyzing the most active compounds (IC_{50} <1 μM) reveals the presence of a hydrophobic region around the substituted benzene ring at the opposite side at a distance of 17.60–18.00 Å from edge (A). Optimal shape and hydrophobicity was also identified in other studies as major physicochemical parameters responsible for high affinity of flavonoid derivatives.[35–37] Furthermore, Cianchetta and co-workers identified the same features at a distance of 20.5 Å apart from each other in selected substrates of P-gp.[38]

In order to further explore the hydrogen bonding related properties, a distance matrix of hydrogen bond acceptors from all three steric hot spots as well as their mutual distances were computed by GRIND descriptors. In some of the compounds edge (A) again represents an anchor point for corresponding distance calculations. Interestingly, two different distance ranges having opposite behavior have been identified. First, compounds with low activity values show a hydrogen bond acceptor at a distance of 1.60–2.00 Å from a steric hot spot (Fig. 5d). In contrast, both features far apart (20.80–21.20 Å) from each other is seen in the most active compounds (IC_{50} <1 μM) (Fig. 5e). This indicates that potent P-gp inhibitors show an elongated structure and have a hydrogen bond acceptor far from the edges of the molecules.

The number and pattern of H-bond acceptor groups is a subject of various publications. Seelig defined two patterns of H-bond acceptors and proposed that P-gp ligands may contain two or more H-bond acceptors which are separated either 2.5 ± 0.3 Å and/or 4.6 ± 0.6 Å apart from each other.[39,40] Interestingly, no consistency has been observed in the distance profile between different pairs of H-bond acceptors in chalcone derivatives. A distance of 9.20–9.60 Å has been identified between two carbonyl groups of **20**–**23** and between one carbonyl group and a region between the 6- and 7-methoxy group of the highly active indanone derivative **10** (IC_{50}: 0.04 μM) (Fig. 5f). However, this distance is not consistently present in all compounds having IC_{50} values <1 μM. Interestingly, a similar distance (8.80–9.20 Å) has been found to be important for activity of conformationally rigid benzopyrano[3,4*b*][1,4]oxazine-type inhibitors of P-gp.[41] In another study, performed on flavonoid derivatives, a distance of 8.00 Å between

Table 2
GRID-independent descriptors that are highly correlated to biological activity of chalcone derivatives **3**–**24**

Variable	Distance	Correlogram	Comment
40	16.00–16.40 Å	DRY-DRY	Represents two large hydrophobic groups, remains highly consistent throughout the length of the correlogram
292	22.00–22.40 Å	TIP-TIP	Distance between two steric hot spots of the molecule
518	17.60–18.00 Å	DRY-TIP	Distance of a hydrophobic group to one particular steric hot spot
715	1.60–2.00 Å	N1-TIP	Distance between a hydrogen bond acceptor and a steric hot spot , showing negative contribution to biological activity
763	20.80–21.20 Å	N1-TIP	Distance between a hydrogen bond acceptor and a steric hot spot, showing beneficial contribution to potency
442	18.80–19.20 Å	DRY-N1	Distance between one of the two hydrophobic moieties to a hydrogen bond acceptor

two H-bond acceptors has been linked to high P-gp inhibitory activity.[42] A slightly larger distance (11.5–15 Å) has been identified by Cianchetta and co-workers,[38] for substrates of P-gp. Finally, a similar distance range between two H-bond acceptors has been proposed by Pajeva et al., for a diverse data set of P-gp substrates/inhibitors, which are supposed to interact with the verapamil binding site.[43]

Although some similarities in mutual distances between two H-bond acceptors seem to exist, there is still an inconsistent picture and no clear threshold for efficient separation of more potent P-gp inhibitors from least active ones. This most probably reflects the notion that the large binding site in P-gp offers numerous possibilities to contribute to hydrogen bond driven interactions and thus allows a series of distinct, but different binding modes.

4. Conclusion

With the current study we present a series of novel chalcone derivatives which in part show P-gp inhibitory activity in the nanomolar range. Based on a set of 22 compounds covering different modifications of the chalcone scaffold, two predictive QSAR models were established in order to elucidate the molecular features responsible for high biological activity. 2D-QSAR analysis revealed the importance of the hydrophobic surface area and the number of rotatable bonds. Interestingly, in contrast to several other compound classes, there was only a poor correlation between overall lipophilicity of the compounds and their P-gp inhibitory activity. This indicates that for chalcones hydrophobic areas directly contribute to ligand binding. This is further exemplified by the GRIND analysis, which identified three hydrophobic hot spots in the molecules. Furthermore, distinct distances between these hydrophobic features and H-bond acceptors have been exemplified. Remarkably, these compounds do not contain a basic nitrogen atom. Furthermore, they exhibit a quite rigid and planar structure, which renders them quite unique in the chemical space of P-gp inhibitors. Thus, chalcones represent an interesting new class of P-gp ligands which will deserve further investigation.

Acknowledgements

We acknowledge Austrian Science Foundation, grants F3502 and F3509 for financial support and Higher Education Commission Pakistan for giving scholarship to Z.P. and I.J. to complete this study.

References and notes

1. Loo, T. W.; Clarke, D. M. *Arch. Biochem. Biophys.* **2008**, *476*, 51.
2. Gottesman, M. M.; Hrycyna, C. A.; Schoenlein, P. V.; Germann, U. A.; Pastan, I. *Annu. Rev. Genet.* **1995**, *29*, 607.
3. Kruijtzer, C. M. F.; Beijnen, J. H.; Rosing, H.; ten Bokkel Huinink, W. W.; Schot, M., et al *J. Clin. Oncol.* **2002**, *20*, 2943.
4. Klepsch, F.; Jabeen, I.; Chiba, P.; Ecker, G. F. *Curr. Pharm. Des.* **2010**, *16*, 1742.
5. Zhang, S.; Yang, X.; Coburn, R. A.; Morris, M. E. *Biochem. Pharmacol.* **2005**, *70*, 627.
6. Zhang, S.; Morris, M. E. *J. Pharmacol. Exp. Ther.* **2003**, *304*, 1258.
7. Sheu, M.-T.; Liou, Y.-B.; Kao, Y.-H.; Lin, Y.-K.; Ho, H.-O. *Chem. Pharm. Bull.* **2010**, *58*, 1187.
8. Boumendjel, A.; McLeer-Florin, A.; Champelovier, P.; Allegro, D.; Muhammad, D., et al *BMC Cancer* **2009**, *9*, 242.
9. Han, Y.; Riwanto, M.; Go, M.-L.; Rachel Ee, P. L. *Eur. J. Pharm. Sci.* **2008**, *35*, 30.
10. Liu, X. L.; Tee, H. W.; Go, M. L. *Bioorg. Med. Chem.* **2008**, *16*, 171.
11. Joshi, B. P.; Sharma, A.; Sinha, A. K. *Tetrahedron* **2005**, *61*, 3075.
12. Barnes, R. P.; Cochrane, C. C. *J. Am. Chem. Soc.* **1942**, *64*, 2262.
13. Xu, W.-Z.; Huang, Z.-T.; Zheng, Q.-Y. *J. Org. Chem.* **2008**, *73*, 5606.
14. Charonnet, E.; Filippini, M. H.; Rodriguez, J. *Synthesis* **2001**, 0788.
15. Chiba, P.; Ecker, G.; Schmid, D.; Drach, J.; Tell, B., et al *Mol. Pharmacol.* **1996**, *49*, 1122.
16. Durán, Á, Pastor, M. Pentacle An Advanced Tool for Computing and Handling GRid-INdependent Descriptors. User manual version 0.9. User manual version 09.
17. Duran, A.; Martinez, G. C.; Pastor, M. *J. Chem. Inf. Model.* **2008**, *48*, 1813.
18. Clementi, M.; Clementi, S.; Cruciani, G.; Pastor, M. Chemometric Detection of Binding Sites of 7TM Receptors. In *Molecular Modelling and Prediction of Bioreactivity*; Gundertofte, K., Jorgensen, F. S., Eds.; Kluwer Academic/Plenum Publishers: New York, 2000; pp 207–212.
19. *Molecular Operating Environment (MOE)*, Chemical Computing Group: Quebec, Canada, 2010.
20. Seelig, A. *Eur. J. Biochem.* **1998**, *251*, 252.
21. Biot, C.; Glorian, G.; Maciejewski, L. A.; Brocard, J. S.; Domarle, O., et al *J. Med. Chem.* **1997**, *40*, 3715.
22. Huber, D.; Hübner, H.; Gmeiner, P. *J. Med. Chem.* **2009**, *52*, 6860.
23. Hogg, R. V.; Tanis, E. A. *Probability and Statistical Inference*; Macmillan Publishing: New York, 1993.
24. Wang, R. B.; Kuo, C. L.; Lien, L. L.; Lien, E. J. *J. Clin. Pharm. Ther.* **2003**, *28*, 203.
25. Wiese, M.; Pajeva, I. K. *Curr. Med. Chem.* **2001**, *8*, 685.
26. Chiba, P.; Holzer, W.; Landau, M.; Bechmann, G.; Lorenz, K., et al *J. Med. Chem.* **1998**, *41*, 4001.
27. Hiessbock, R.; Wolf, C.; Richter, E.; Hitzler, M.; Chiba, P., et al *J. Med. Chem.* **1999**, *42*, 1921.
28. Pleban, K.; Hoffer, C.; Kopp, S.; Peer, M.; Chiba, P., et al *Arch. Pharm. (Weinheim)* **2004**, *337*, 328.
29. König, G.; Chiba, P.; Ecker, G. F. *Monatsh. Chem. Chem. Mon.* **2008**, *139*, 401.
30. Aller, S. G.; Yu, J.; Ward, A.; Weng, Y.; Chittaboina, S., et al *Science* **2009**, *323*, 1718.
31. Pastor, M.; Cruciani, G.; McLay, I.; Pickett, S.; Clementi, S. *J. Med. Chem.* **2000**, *43*, 3233.
32. Gasteiger, J.; Rudolph, C.; Sadowski, J. *Tetrahedron Comput. Methodol.* **1990**, *3*, 537.
33. Durán, Á.; Pastor, M. *An Advanced Tool for Computing and Handling GRid-INdependent Descriptors. User Manual Version 1.06*, 2011
34. Broccatelli, F.; Carosati, E.; Neri, A.; Frosini, M.; Goracci, L., et al *J. Med. Chem.* **2011**, *54*, 1740–1751.
35. Boccard, J.; Bajot, F.; Di Pietro, A.; Rudaz, S.; Boumendjel, A., et al *Eur. J. Pharm. Sci.* **2009**, *36*, 254.
36. Boumendjel, A.; Beney, C.; Deka, N.; Mariotte, A. M.; Lawson, M. A., et al *Chem. Pharm. Bull. (Tokyo)* **2002**, *50*, 854.
37. Boumendjel, A.; Di Pietro, A.; Dumontet, C.; Barron, D. *Med. Res. Rev.* **2002**, *22*, 512.
38. Cianchetta, G.; Singleton, R. W.; Zhang, M.; Wildgoose, M.; Giesing, D., et al *J. Med. Chem.* **2005**, *48*, 2927.
39. Seelig, A. *Eur. J. Biochem.* **1998**, *251*, 252.
40. Seelig, A. *Int. J. Clin. Pharmacol. Ther.* **1998**, *36*, 50.
41. Jabeen, I.; Wetwitayaklung, P.; Chiba, P.; Pastor, M.; Ecker, G. F. *Eur. J. Med. Chem.* **2011**. submitted article.
42. Crivori, P.; Reinach, B.; Pezzetta, D.; Poggesi, I. *Mol. Pharm.* **2006**, *3*, 33.
43. Pajeva, I. K.; Wiese, M. *J. Med. Chem.* **2002**, *45*, 5671.